Executive Summary

CAER

By 1950, it was recognized that a simple polymerization mechanism should describe the Fischer-Tropsch synthesis product distribution, the so-called Anderson-Schulz-Flory (ASF) distribution. Thus, a plot of the logarithm of the molar concentration versus the carbon number would produce a straight line plot whose slope is related to alpha, the chain propagation probability. While this description has become widely accepted, it was also recognized at that time that the actual products, when higher carbon-number products were included, could not be described by a single alpha value. The so-called two-alpha distribution of products from several larger-scale plants in Germany and the U.S. were demonstrated in a plots by Anderson. In each of these and subsequent plots it has been shown that the break occurs in the range of carbon numbers 8 to 14.

Several models have been proposed to account for the two, or even more, alpha values. One that is frequently cited is the operation of two or more chains that undergo propagation independently. Another reason frequently cited for the two alpha distribution is the impact of diffusion and reincorporation of higher carbon number alkenes. It has become apparent that the ^{14}C-distribution in the products when labeled alcohols or alkenes are added to the synthesis gas fed to a continuous stirred tank reactor (CSTR) are impacted by accumulation of heavier products in the liquid in the reactor. Bell, among others, has shown that the initial gas phase products are depleted of higher carbon number products during the Fischer-Tropsch synthesis in a CSTR. For a catalyst that exhibits a constant conversion for some period and then declines in activity, the accumulation effects can provide a two alpha plot since the increasing gas flow carries accumulated products from the reactor in higher concentrations than they are formed. It was therefore of interest to learn whether a two alpha plot could be obtained when a catalyst with constant activity was utilized in a slurry reactor. Results of calculations for vapor-liquid equilibrium models corresponding to the operation of a Fischer-Tropsch catalyst with a single alpha value was utilized in a CSTR are provided in this manuscript.

Filtration results for the CAER are summarized below:

Summary of Filtration with Iron and Cobalt Catalysts			
Alpha	**Iron, Unsupported**	**Iron, Supported**	**Cobalt, Supported**
Low (< ≈ 0.7)	No Problem	No Problem	---
Intermediate (0.7 to 0.85)	Problems in some runs	-----	No Problem
High (> 0.85)	Problems	Problems	No Problem

UC/B

During this reporting period, X-ray absorption measurements were carried out at the Stanford Synchrotron Radiation Laboratory (SSRL). We measured potassium K-edge spectra of Fe-Zn-K-Cu oxides and their carbides. We also measured *in-situ* Fe K-edge spectra of a typical

Fe-Zn-K-Cu oxide (Zn/Fe=0.1, K/M=0.02, Cu/M=0.01, M=(Fe+Zn)) during the reduction in H_2, and during the reduction and carburization in CO and in synthesis gas.

Potassium K-edge X-ray absorption near edge structure (XANES) spectra of Fe-Zn-K-Cu oxides and their carbides showed that K was well dispersed on Fe and Zn oxides rather than present as K_2CO_3, while K was present as K_2CO_3 in the carburized samples. For Fe-Zn-K-Cu oxides, beyond the pre-edge (7.113 keV), the Fe K-edge XANES showed the absorption energy at 7.123 keV, indicating the presence of low oxidation state species like FeO besides the predominant Fe_2O_3 species. *In-situ* Fe K-edge XANES of Fe-Zn-K-Cu oxides in CO at temperature up to 500°C showed that Fe carbides had an absorption energy at 7.112 keV. The EXAFS spectra confirmed the Fe-Fe distance in carbides at 2.0 Å. *In-situ* Fe K-edge XAS spectra of Fe-Zn-K-Cu oxides in synthesis gas at 270°C showed that Fe carbides were formed in the dominant bulk Fe oxides, and that the extent of carburization increased with increasing space velocity and time on stream.

We have also continued to investigate the effects of K and Cu on Fe-catalyzed FTS reactions. The effects of K on secondary hydrogenation and isomerization reactions of primary α-olefins formed during FTS were examined on Fe-based catalysts (Zn/Fe=0.1, Cu/M=0.01) with different K contents (K/M=0-0.04). Fe-Zn-Cu catalysts were active for secondary hydrogenation and isomerization reactions of α-olefins. The introduction of K titrated these active sites. At 235℃, the K-free catalyst was active for secondary reactions while K-promoted catalysts showed no activity for these reactions. At 270°C, these K-promoted catalysts became active for secondary reactions but their activities were much lower than for the K-free catalyst.

The effects of Cu on the activities for FTS and WGS reactions were examined on Fe-based catalysts (Zn/Fe=0.1, K/M=0.02) with varying Cu loading (Cu/M=0-0.04). The addition of Cu increased FTS and WGS activities. Further addition of Cu to Fe-based catalysts (Cu/M=0.02) had no additional promotion effects. In addition, the promotion effects of Cu on these activities were less marked than those observed for K. The addition of Cu to Fe-based catalysts had little effect on hydrocarbon productions and olefin selectivities.

In this quarter, the study of cobalt-based FTS was continued with focus on the reaction mechanism. The D_2-H_2 exchange, which was carried out under FTS conditions, showed that HD formation rates were much higher than the corresponding rates of hydrogen conversion to hydrocarbons (almost 20 times higher at zero CO conversion). This indicated that the H_2 dissociation step was reversible and quasi-equilibrated in FTS. D_2O tracer studies showed that the deuterium content in the H_2 isotopomers and hydrocarbons increased with increasing bed residence time. This indicated that water dissociation proceeded slowly and was not quasi-equilibrated during FTS on Co-based catalysts. The observed positive effect of water on the synthesis rate and C_{5+} selectivity can be explained if surface C* reacted with both H* and OH_2*. The latter pathway was affected by the partial pressure of gas phase water. Combined with the results of D_2-H_2 exchange and D_2O tracer experiments, we proposed a mechanism for the overall CO conversion.

1. $H_2 + 2* \leftrightarrow 2H*$
2. $CO + 2* \leftrightarrow C* + O*$
3. $C* + H* \rightarrow CH* + *$
4. $C* + OH* \rightarrow COH* + *$
5. $O* + H* \rightarrow OH* + *$
6. $OH* + H* \rightarrow OH_2* + *$
7. $OH_2* \leftrightarrow H_2O + *$

Applying the pseudo-steady state approximation through step 1 to step 7, we obtained a Langmuir-Hinshelwood type rate expression: $r_{-CO} = aP_{CO}^{1/2}P_{H2}^{1/4}(bP_{H2}^{1/2} + cP_{H2O})^{1/2}/(1 + dP_{H2}^{1/2} + eP_{H2O} + fP_{CO}^{1/2})^2$, where a, b, c, d, e, and f are temperature-dependent kinetic or thermodynamic parameters. The reaction kinetics of FTS was studied on a Co/SiO_2 catalyst over a wide range of reaction pressures and $H_2/CO/H_2O$ ratios. This data will be regressed nonlinearly and fitted to a Langmuir-Hinshelwood type rate expression, which will be more representative of the true FTS mechanism on cobalt-based catalysts.

Task 1. Iron Catalyst Preparation

The objective of this task is to produce robust intermediate- and high-α catalysts.

The effects of heat and gas composition on volume change of an unpromoted iron catalyst was studied using visual examination of a catalyst bed in a 1 inch diameter Pyrex tube.

Iron oxide pellets were prepared by precipitation of aqueous $Fe(NO_3)_3$ with NH_4OH (same preparation method used for RLS001). The gel was washed with at least seven volumes of distilled deionized water to remove excess NH_4 then extruded to form cylindrical pellets approximately 3 mm in diameter and 1 to 1.5 cm in length. The pellets were dried overnight at 120°C and calcined in a muffle furnace at 350°C for 8 hours. The catalyst was held in the center of the tube between glass wool plugs forming a bed approximately 3 cm long. The reactor tube was heated in a shell furnace controlled by a thermocouple inserted in the catalyst bed and video recordings were made at various points during heating to allow measurement of the pellets.

Initially the reactor was heated to 270°C in H_2/CO flow (H_2:CO = 0.42). Inspection after 1 hr. Showed no changes; however, after 24 hr. A shiny silver colored deposit was observed on the glass wool and inside wall of the Pyrex tube upstream from the catalyst bed. The charge was removed and attempts to clean the tube by scrubbing and heating proved unsuccessful; only soaking in aqua regia and subsequent washing removed the deposit. Analysis of the film identified it as an X-ray amorphous material consisting of C and Fe.

A number of changes were made to the system in an effort to eliminate the deposition of including: replacement of glass wool and beads with stainless steel screens to maintain the shape of the catalyst bed, changing from Pyrex to a quartz reactor tube, heating an inert gas before admitting H_2/CO or pure CO, diluting the CO stream with N_2, testing the furnace for "hot spots", carefully washing to remove all traces of catalyst fines upstream of the bed, reducing the temperature and finally heating the empty tube in flowing CO. In all cases the formation of a carbonaceous deposit on the inside of the reactor was observed at temperatures as low as 150°C even when empty. As a result, this method of measuring change in catalyst volume was determined to be unsuccessful.

Task 2. Catalyst Testing

The objective of this task is to obtain catalyst performance on the catalysts prepared in Task 1.

Two Alpha Fischer-Tropsch Product Distribution. A Role for Vapor Liquid Equilibrium?

Abstract

The simple polymerization mechanism for the Fischer-Tropsch synthesis produces products which follows an Anderson-Schulz-Flory distribution. Thus, plotting the logarithm of the mole fraction versus carbon number will produce a straight line whose slope is related to alpha which is determined by the chain termination and propagation probabilities. In contrast, the products from laboratory and large commercial plants exhibit a two-alpha plot. Vapor-liquid calculations show that product accumulation cannot be responsible for the two-alpha plot when the alpha value is large enough to produce liquid products at the reaction temperature. Only in

the case where alpha is small and all products are in the vapor phase, allowing evaporation of the startup solvent and a "drying out" of the reactor can a product accumulation produce a two-alpha plot.

Introduction

By 1950, it was recognized that a simple polymerization mechanism should describe the Fischer-Tropsch synthesis product distribution, the so-called Anderson-Schulz-Flory (ASF) distribution (1-3). Thus, a plot of the logarithm of the molar concentration versus the carbon number would produce a straight line plot whose slope is related to alpha, the chain propagation probability. While this description has become widely accepted, it was also recognized at that time that the actual products, when higher carbon-number products were included, could not be described by a single alpha value. The so-called two-alpha distribution of products from several larger-scale plants in Germany and the U.S. were demonstrated in a plots by Anderson (4). In each of these and subsequent plots it has been shown that the break occurs in the range of carbon numbers 8 to 14.

Several models have been proposed to account for the two, or even more, alpha values (5). One that is frequently cited is the operation of two or more chains that undergo propagation independently (6-8). Another reason frequently cited for the two alpha distribution is the impact of diffusion and reincorporation of higher carbon number alkenes (9-14). It has become apparent that the ^{14}C-distribution in the products when labeled alcohols or alkenes are added to the synthesis gas fed to a continuous stirred tank reactor (CSTR) are impacted by accumulation of heavier products in the liquid in the reactor (15). Bell, among others, has shown that the initial gas phase products are depleted of higher carbon number products during the Fischer-Tropsch synthesis in a CSTR (16). For a catalyst that exhibits a constant conversion for some period and then declines in activity, the accumulation effects can provide a two alpha plot since the increasing gas flow carries accumulated products from the reactor in higher concentrations than they are formed (17). It was therefore of interest to learn whether a two alpha plot could be obtained when a catalyst with constant activity was utilized in a slurry reactor. Results of calculations for vapor-liquid equilibrium models corresponding to the operation of a Fischer-Tropsch catalyst with a single alpha value was utilized in a CSTR are provided in this manuscript.

Continuous Stirred Tank Reactor

The continuous stirred tank reactor provides the advantage that all catalyst particles have the same average catalyst life (based on usage), all catalyst particles are exposed to the same synthesis gas composition, and the reaction temperature is uniform in the catalyst slurry. Thus, the typical CSTR for Fischer-Tropsch synthesis is operated under constant temperature, pressure and reactant compositions. A certain amount of paraffin is charged to the reactor as starting solvent to provide a slurry phase. Reactant gases, i.e., CO and H_2, continuously flow into the reactor at constant rates. Vapor phase products, i.e., unconverted CO and H_2, CO_2, water, and volatile hydrocarbons, continuously flow out. Liquid phase products are either removed continuously or allowed to accumulate in the reactor for some time interval. In the latter mode of operation, the excess reactor liquid is drained periodically, as necessary, so that the reactor is operated at a nearly constant liquid level. The drained liquid is added to the vapor phase product to obtain the total reaction product for the sampling period.

For the development of VLE model for Fischer-Tropsch synthesis, it is convenient to divide a CSTR reactor into two operational parts, i.e., reaction and separation, as illustrated schematically in Figure 1, where,

F_{CO}, F_{H_2}, F :	molar flow rate of feed CO, feed H_2, and total flow after reaction, respectively
X_{CO} :	CO conversion to hydrocarbons
x_i, y_i, z_i:	individual hydrocarbon molar fraction in reactor slurry, vapor stream, and the combined streams after reaction, respectively
k_i :	vapor-liquid equilibrium constant
L:	moles of reactor liquid
V:	molar flow rate of vapor stream

Fischer-Tropsch Reaction

For the Fischer-Tropsch reaction, it is assumed that CO and H_2 react stoichiometrically to produce hydrocarbons (exclusively paraffins for simplicity) and water following a single α ASF distribution and constant catalyst activity. Also, the fraction of CO converted to hydrocarbons (X_{CO}) is assumed to be constant through any reaction time period. Therefore, with constant reactant flow rates, the total flowrate of the stream after reaction (F) is constant. In addition, the each component in the reactor effluent (z_i) is constant with time. The water gas shift reaction, which is significant with an iron catalyst, is not included explicitly in this model because it is an equal molar reaction that does not impact the total reactor effluent flow. This reaction does not affect hydrocarbon product distribution if the gases are insoluble, or of limited solubility, in the reactor liquid.

Based on the above assumptions, the Fischer-Tropsch reaction can be written as

$$(2n+1)\ H_2 + n\ CO \rightarrow C_nH_{2n+2} + nH_2O \quad (\ n = 1/(1-\alpha)\ ) \tag{1}$$

and the composition of each hydrocarbon produced by the reaction

$$Z_i = (1-\alpha)^2\ \alpha^{i-1}\ F_{co}\ X_{co} / F \tag{2}$$

Vapor-Liquid Separation

In the vapor-liquid separation component, the input is the stream leaving the reaction component. Here, the input stream is separated into liquid and vapor, which are assumed to be in thermodynamic equilibrium at reaction temperature and pressure (Eq. (3)). Equations (4) and (5) are used to describe the material balance for the separation process.

$$y_i = k_i x_i \tag{3}$$

$$\frac{dL}{dt} = F - V \tag{4}$$

$$\frac{d(Lx_i)}{dt} = Fz_i - Vy_i \tag{5}$$

The above equations can be solved numerically. For an infinitesimally small time interval, Δt, equations (3) - (5) can be combined to give

$$x_i = \frac{Fz_i\Delta t + (Lx_i)_{prev}}{L + k_i(F\Delta t - L + L_{prev})} \tag{6}$$

Equation (6) allows the calculation of the composition, x_i, and amount, L, of liquid in the reactor at any time interval within the constraint of Equation (7).

$$\Sigma x_i = 1 \tag{7}$$

With a knowledge of the initial reaction conditions, the liquid composition, vapor composition, vapor flow rate, and the amount of liquid in the reactor can be calculated at any time-on-stream.

Model Simulation

Based on the above model, the simulation is performed using a computer program developed in our lab. For simplicity of simulation, it was further assumed that hydrocarbon products are linear paraffins from C_1 to C_{100} whose relative concentrations follow a single α ASF distribution. Also for simplicity, CO, H_2, and H_2O are assumed to be insoluble in reactor liquid. All vapors are assumed to be idea gases and the liquid is assumed to be an idea solution; their compositions are related by Roult's law:

$$y_i = k_i x_i = \frac{P_i^s}{P} x_i \tag{8}$$

In the simulations, unless noted otherwise, the saturation vapor pressures of the Caldwell and Van Vuuren paraffins in Equation (8) are calculated using Equation (9) obtained from the literature (18). In this correlation, the unit for vapor pressure is atm and the unit for temperature is Kelvin.

$$P_i^s = 176.0452\exp(-427.218(\frac{1}{T} - 1.029807\times 10^{-3})) \tag{9}$$

The paraffin vapor pressure was also estimated using Antoine's equation whose constants are obtained from API Project 44 (19). The difference between vapor pressure from these two sources and their impact on FT product distribution will be discussed later. A temperature dependent correlation from the literature (20) is used to estimate the partial molar volumes of paraffins in the FT liquid. Other conditions for simulation are Newton's method for iteration of Equation (6), accuracy of the sum of liquid molar fraction of 0.0001 (Eq. (7)), and time interval of 0.01h for each numerical calculation.

Before reaction, a certain amount of C_{28} paraffin is added to the reactor as start-up solvent. This volume is used as the liquid volume to be maintained in the reactor. The catalyst volume is ignored in this simulation. The reaction effluent enters the separator, with vapor

products leaving continuously and liquid products accumulating for some time interval. The amount of liquid in the reactor is examined at each time interval. If the liquid level is higher than that to be maintained, the extra volume is drained instantaneously so that the liquid level is constant throughout the simulation. The liquid drained from the reactor, if there is any, is added to the vapor stream as the total reaction products generated during that sampling period. Vapor products collected include water, unconverted H_2 and CO, and hydrocarbons. The flowrate of the vapor stream and its compositions are normalized to those of pure hydrocarbons for further calculations. Since C_{28} paraffin is used as the start-up solvent, its composition in both liquid and vapor are substantially higher than they should be in the Fischer-Tropsch product. Therefore, C_{28} is removed from vapor product as it does not represent what is produced by the reaction. Its composition in the vapor is determined from the amount of C_{27} and C_{29} using single α distribution rule. The same method is used for the liquid which is drained from the reactor and is added to the vapor stream to obtain the total reaction product.

The following seven (7) parameters are required as input to the simulation program: reaction temperature (°C), reaction pressure (atm), H_2 flowrate (SL/h), CO flowrate (SL/h), CO conversion (mole%), amount of C_{28} starting solvent (g), and the single α value.

Simulation Results

Two sets of reaction conditions are used to illustrate the effect of VLE on the FT product distribution. The common conditions are temperature (270°C), pressure (12.9 atm), hydrogen flow rate (F_{H_2}; 23 SL/h), CO flow rate (F_{CO}; 33 SL/h), conversion of CO to hydrocarbons (X_{CO}; 40%), and the amount of C_{28} starting solvent (300g). The only difference is single α value; α=0.85 represents normal operating condition with liquids accumulation and α=0.65 which represents a drying out condition due to excessive evaporation of the starting solvent.

Figures 2 through 4 shows the hydrocarbon product distribution with an α value of 0.85 when the reactor is operated under normal conditions without drying out. In Figure 2 and the liquid phase plots thereafter, the composition of starting solvent (C_{28}) is not shown since it is not representative. The composition of a hydrocarbon in both liquid phase (Figure 2) and vapor phase (Figure 3) increases with time-on-stream before leveling off. The higher the carbon number, the longer time-on-stream it takes to attain the "steady-state" composition. After 5000 hours on stream, both liquid and vapor compositions become stable and are no longer affected by reaction time. For vapor phase composition, there is always a negative deviation from the ASF distribution for about C_{20}+ products, due to the thermodynamic effect. When the drained reactor liquid is added to the vapor stream to obtain the total reaction product, as shown in Figure 4, the product distribution approaches a single α distribution, although there is still a negative deviation before steady state. Also shown in Figure 4 are two dashed lines for liquid and vapor phases at 100 h to illustrate how they are combined to generate the total reaction product distribution. Once the reactor reaches steady state, the total reaction product distribution is represented by a single α distribution and without deviation. Longer reaction times up to 10,000 hours do not change this distribution. It appears that, with a single α chemistry, vapor/liquid separation and/or accumulation is not responsible for the two α observation.

Figures 5 and 6 show the simulation results with α=0.65 when the reactor is drying-out at 508 h due to excessive evaporation of the start-up solvent. The vapor stream is the only product collected since the reactor liquid level decreases with time-on-stream, and hence no liquid can be drained from the reactor. As shown in Figure 5, the hydrocarbon fraction in the reactor liquid decreases with carbon number except when the reactor is close to drying-out, in contrast to

normal operation (Figure 2) in which liquid fraction increases with carbon number and then decreases after reaching a maximum. Figure 6 shows the vapor phase composition, together with the theoretical ASF plot (dotted line). It is interesting to note that after some time on stream (e.g., 400 h), the vapor composition begins to show positive deviation from the ASF distribution. Obviously, this is due to the flashing-off of previously-accumulated heavier hydrocarbons, in agreement with earlier observations (17). Misinterpretation of this phenomena may lead to the conclusion of a two α product distribution. It should be noted that, with single α chemistry, positive deviation is possible only under drying-out conditions. Under the extreme situation when the reactor is dry (508 h, liquid level 0.1% of initial level in this simulation), an abnormal phenomena occurs. The plot at this time on stream indicates that the α value can be larger than unity over a range of carbon numbers, which is impossible from the chemical reaction stoichiometry.

As mentioned previously, a correlation from the literature is used to calculate the paraffin vapor pressure for vapor/liquid separation. Data from other sources may lead to different product distribution. Figure 7 compares the differences for the paraffin vapor pressure at 270°C from two sources, the one used in this simulation and the other one from API Project 44 (19). For carbon numbers higher than about 40, the vapor pressure deviates from each other, and the deviation becomes greater with increasing carbon number. As a result, predicted product distribution in both vapor phase and liquid phase depend on the data used. For the example shown in Figure 8, vapor pressure from API Project 44 predicts higher concentration of C_{30+} paraffins in the vapor phase, and a lower concentration in liquid phase. However, when the reactor reaches "steady-state", the total reaction product distribution is represented by a single α straight line. The dependence of vapor and liquid on vapor pressure is canceled out when the drained liquid is added to the vapor to produce the total reaction product. It is therefore reasonable to predict that as long as the reactor is operated under normal conditions, the total reaction product distribution is independent of the vapor-liquid equilibrium constant (k value), although vapor and liquid compositions will vary.

Conceptual Illustration

The above discussion is based on computer simulation involving 100 components with assumptions such as ideal gases, idea solution, and vapor/liquid separation at equilibrium. In fact, whether two α observation in FT synthesis can, or cannot, be attributed to vapor-liquid separation can be understood conceptually from separation principles.

A binary system shown in Figure 9 is used to illustrate the composition change with time. Pure component A continuously flows into the tank initially containing A_0 amount of A and B_0 amount of non-volatile component B. The objective is to examine if there is any chance that the amount of A in the output (vapor + drained liquid) be more than its input, due to accumulation of A in the liquid phase over time. A positive answer will lead to the vapor/liquid separation being responsible for the two α product distribution in the FT synthesis.

For easier discussion, it is assumed that the liquid phase density is constant so that its volume is directly proportional to its mass. The vapor phase and liquid phase are not necessarily in equilibrium, nor do they need to be an idea mixture. This binary separation process can be described as:

1) During any time interval Δt_i (t_i - t_{i-1}) , F amount of A flows in, V_i amount of A flows out, and Δ_i is the amount of A leftover in the liquid phase.

2) Vapor flows out continuously, but the liquid level might increase due to accumulation of A. The liquid is drained to the level of L_0 instantaneously or at time t_n , if L_n is higher than L_0.

These two liquid draining cases will be discussed separately in the following section.

Liquid Allowed to Accumulate over a Time Period This is the most common operation practice for FT synthesis in a CSTR. Typically, exit vapor is collected in a condenser vessel during the sampling period, e.g., each 24 hours. The reactor liquid level is allowed to increase during this period before draining the reactor to the desired level. The drained reactor liquid is then added to the vapor condensate to obtain the total reaction product for this period. Therefore, the product distribution is actually the average of the sampling period. For the binary system discussed here, the sampling period is divided into **n** time intervals, each being of differential scale theoretically. The amount of A in vapor and liquid at each time interval is shown in Table 1. At the end of the sampling period, t_n, the reactor liquid is drained to the initial level of L_0. The total amount of A in output (F_{out}) is the sum of A in the drained liquid and the amount of A in vapor, shown as follows:

Total component A collected in vapor phase: $V = \sum V_i = nF - \sum \Delta_i = F_{in} - \sum \Delta_i$
Total component A drained from liquid phase:
$L = (L_n - L_0)C_n = (\sum \Delta_i) (A_0 + \sum \Delta_i)/(L_0 + \sum \Delta_i)$
Total A sampled

$$\begin{aligned} F_{out} &= V + L \\ &= F_{in} - \Sigma\Delta_i + \frac{(\Sigma\Delta_i)(A_0 + \Sigma\Delta_i)}{L_0 + \Sigma\Delta_i} \\ &= F_{in} - \frac{B_0 \cdot \Sigma\Delta_i}{L_0 + \Sigma\Delta_i} \end{aligned} \qquad (10)$$

In Equation (10), F_{in} and F_{out} are the input and output of A during the sampling period, respectively. The amount of A in output depends on the following four cases:

1) $\sum \Delta_i > 0$, $F_{out} < F_{in}$, accumulation of A in liquid phase, negative deviation
2) $\sum \Delta_i = 0$, $F_{out} = F_{in}$, no accumulation of A in liquid phase, single α observation
3) $\sum \Delta_i < 0$ & $(-\sum \Delta_i) < L_0$, $F_{out} > F_{in}$, drying-out, false two α observation
4) $\sum \Delta_i < 0$ & $(-\sum \Delta_i) \hookrightarrow L_0$, $F_{out} \hookrightarrow \infty$, almost dry, hump observed, $\alpha > 1$

Case 1 is an unsteady state process for component A which accumulates in the separation tank. In FT synthesis, product distribution will show negative deviation from ASF distribution in this case. Case 2 is a "steady state" when the amount of A that accumulates during the sampling period equals the amount drained so that there is no net accumulation of A. These two cases are under normal operating conditions corresponding to Figure 4 in FT synthesis. In cases 3 and 4, the negative accumulation of A indicates that more material is collected in output than added in the input. This is possible only when the previously accumulated A in the tank is carried out by

the flowing vapor. In FT synthesis, product distribution will exhibit positive deviation from ASF distribution. When the reactor is nearly dry (Case 4), F_{out} in much larger than F_{in}, which explains the "hump" in Figure 6.

Liquid Sampling Instantaneously (constant liquid level)

In this case, liquid level is kept constant by draining extra liquid instantaneously at each time interval. The liquid level is kept at the amount of L_0 after liquid draining. Table 2 shows the material balance of component A at each time interval. Similar to the above example where liquid is allowed to accumulate, the amount of A in output cannot be higher than its input unless under drying out conditions.

Summary

From the above computer simulation and the conceptual discussion, it is concluded that under normal operating conditions, the observation of two α values for the Fischer-Tropsch synthesis cannot be due to VLE of reaction products. A positive deviation from ASF distribution is possible only when the reactor is drying-out. This false two α distribution should not be interpreted as the responsibility of VLE for normal operation.

References

1. R. B. Anderson, H. Friedel and H. H. Scorch, Fischer-Tropsch reaction mechanism involving stepwise growth of carbon chain, J. Chem. Phys., **19**, 313-319 (1951); R. A. Friedel and R. B. Anderson, J. Am. Chem. Soc., **72**, 1212, 2307 (1950).
2. E. F. G. Herington, Chem. Ind. (London), **(1946)**, 347.
3. S. Weller and R. A. Friedel, Isomer distribution in hydrocarbons from Fischer-Tropsch process, J. Chem. Phys., **17**, 801 (1949).
4. R. B. Anderson in "Catalysis," (P. H. Emmett, Ed.) Reinhold Pub. Co., New York, 1956, pp 208, 209.
5. B. H. Davis, The two-alpha value for iron Fischer-Tropsch catalysts: fact or fiction?, ACS Div. Fuel Chem. Preprints, 37, 172 (1992).
6. L.-M. Tau, H. Dabbagh, S. Bao and B. H. Davis, Fischer-Tropsch Synthesis: Evidence for two chain growth mechanisms, Catal. Letters, 7 127 (1990).
7. L. Konig and J. Gaube, The influence of water and of alkali promoter on the carbon number distribution of FT products formed over iron catalysts, Ber. Bunsenges. Phys. Chem. 9l (l987) ll6.
8. T. J. Donnelly, I. C. Yates and C. N. Satterfield, Analysis and prediction of product distributions of the Fischer-Tropsch synthesis, Energy Fuels, 2, 734-739 (1988).
9. E. Iglesia, S. C. Reyes and R. J. Madon; Transport-enhanced alpha-olefin readsorption pathways in Ru catalyzed hydrocarbon synthesis; J. Catal., 129 (1991) 238-256.
10. R. J. Madon, E. Iglesia and S. C. Reyes; Non-Flory product distributions in Fischer-Tropsch synthesis catalyzed by ruthenium, cobalt and iron; ACS Symp. Series, 517 (1993) 383-396.
11. E. Iglesia, S. C. Reyes and S. L. Soled; Reaction-transport selectivity models and the design of Fischer-Tropsch catalysts; "Computer-Aided Design of Catalysts and Reactors," (E. R. Becker and C. J. Pereira, Eds.), Marcel Dekker, Inc., 1992.
12. K. Fujimoto, L. Fan and K. Yoshii; New controlling method for product distribution in Fischer-Tropsch synthesis reaction; Topics in Catal., 2, 259-266 (1995).
13. S.-R. Yan, L. Fan, Z.-X. Zhang, J.-L. Zhou and K. Fujimoto; Effect of 1-olefin addition on supercritical phase Fischer-Tropsch synthesis over Co/SiO_2 catalyst; 14th Ann. Int. Pittsburgh Coal Conf., Proc., 1997.
14. E. W. Kuipers, C. Scheper, J. H. Wilson, I. H. Vinkenburg and H. Oosterbeek; Non-ASF product distributions due to secondary reactions during Fischer-Tropsch synthesis; J. Catal., 158 (1996) 283-300.)
15. B. Shi, L.-M. Tau, H. Dabbagh, J. Halasz and B. H. Davis, submitted.
16. D. Stern, A. T. Bell and H. Heinemann; Experimental and theoretical studies of Fischer-Tropsch synthesis over ruthenium in a bubble-column reactor; Chem. Eng. Sci., 40 (1985) 1917-1924.
17. A. P. Raje and B. H. Davis, Effect of vapor-liquid equilibrium on Fischer-Tropsch hydrocarbon selectivity for a deactivating catalyst in a slurry reactor, Energy & Fuels, 10, 552 (1996).
18. L. Caldwell and D.S. van Vuuren; On the formation and composition of the liquid phase in Fischer-Tropsch reactors; Chem. Eng. Sci., 41 (1986) 89-96.
19. Thermodynamic Research Center, Texas A&M University; Selected values of hydrocarbons and Related compounds; API Project 44, 1983.

20. J.J. Marano and G.D. Holder; Characterization of Fischer-Tropsch liquids for vapor-liquid equilibria calculations; Fluid Phase Equilibria, 138 (1997) 1-21.

Table 1 Amount of Component A at Any Time Interval When the Liquid Is Allowed to Accumulate

Time	A in Vapor	Amount of Liquid Phase	Concentration of A in Liquid Phase
0		L_0	A_o/L_o
t_1	$V_1 = F\text{-}\Delta_1$	$L_1 = L_0 + \Delta_1$	$C_1 = \frac{A_0 + \Delta_1}{L_1} = \frac{A_0 + \Delta_1}{L_0 + \Delta_1}$
t_2	$V_2 = F\text{-}\Delta_2$	$L_2 = L_0 + \Delta_1 + \Delta_2$	$C_2 = \frac{A_0 + \Delta_1 + \Delta_2}{L_2} = \frac{A_0 + \Delta_1 + \Delta_2}{L_0 + \Delta_1 + \Delta_2}$
t_3	$V_3 = F\text{-}\Delta_3$	$L_3 = L_0 + \Delta_1 + \Delta_2 + \Delta_3$	$C_3 = \frac{A_0 + \Delta_1 + \Delta_2 + \Delta_3}{L_3} = \frac{A_0 + \Delta_1 + \Delta_2 + \Delta_3}{L_0 + \Delta_1 + \Delta_2 + \Delta_3}$
. . . . .			
t_i	$V_i = F\text{-}\Delta_i$	$L_i = L_0 + \Delta_1 + \Delta_2 + ... + \Delta_i$	$C_i = \frac{A_0 + \Delta_1 + \Delta_2 + \ldots \Delta_i}{L_i} = \frac{A_0 + \Delta_1 + \Delta_2 + \ldots \Delta_i}{L_0 + \Delta_1 + \Delta_2 + \ldots \Delta_i}$

Table 2 Amount of Component A at Any Time Interval When Liquid Is Drained Instantaneously

Time	A in Vapor	Concentration of A in Liquid Phase	Total A Collected (vapor + drained liquid)
0		A_o/L_o	
t_1	$V_1 = F\text{-}\Delta_1$	$C_1 = \frac{A_0 + \Delta_1}{L_0 + \Delta_1} = 1 - \frac{B_0}{L_0 + \Delta_1}$	$F_1 = V_1 + \Delta_1 C_1$ $F_1 = V_1 + \Delta_1\left(\frac{A_0 + \Delta_1}{L_0 + \Delta_1}\right) = F - \frac{\Delta_1 B_0}{L_0 + \Delta_1}$
t_2	$V_2 = F\text{-}\Delta_2$	$C_2 = \frac{\Delta_2 + \left(\frac{A_0 + \Delta_1}{\Delta_1 + L_0}\right)\cdot L_0}{L_0 + \Delta_2}$ $= 1 - \frac{L_0 B_0}{(L_0 + \Delta_1)(L_0 + \Delta_2)}$	$F_2 = V_2 + \Delta_2 C_2$ $F_2 = F - \Delta_2 + \Delta_2\left(1 - \frac{L_0 B_0}{(L_0 + \Delta_1)(L_0 + \Delta_2)}\right)$ $= F - \frac{\Delta_2 L_0 B_0}{(L_0 + \Delta_1)(L_0 + \Delta_2)}$
t_3	$V_i = F\text{-}\Delta_3$	$C_3 = 1 - \frac{L_0^2 B_0}{(L_0 + \Delta_1)(L_0 + \Delta_2)(L_0 + \Delta_3)}$	$F_3 = F - \frac{\Delta_3 L_0^2 B_0}{(L_0 + \Delta_1)(L_0 + \Delta_2)(L_0 + \Delta_3)}$
. . . . .			
t_i	$V_i = F\text{-}\Delta_i$	$C_i = 1 - \frac{L_0^{i-1} B_0}{(L_0 + \Delta_1)(L_0 + \Delta_2)\cdots(L_0 + \Delta_i)}$	$F_i = F - \frac{\Delta_i L_0^{i-1} B_0}{(L_0 + \Delta_1)(L_0 + \Delta_2)\cdots(L_0 + \Delta_i)}$

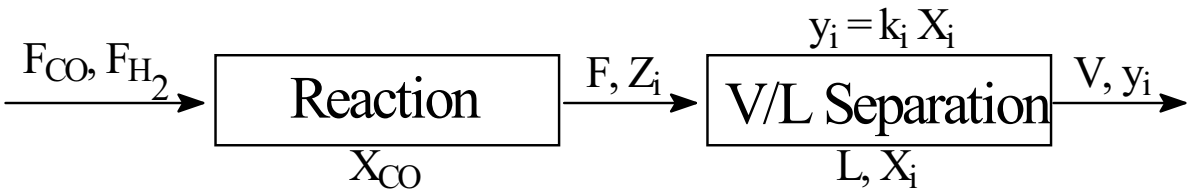

Figure 1. Schematic diagram of VLE mode for Fischer-Tropsch Synthesis in a CSTR.

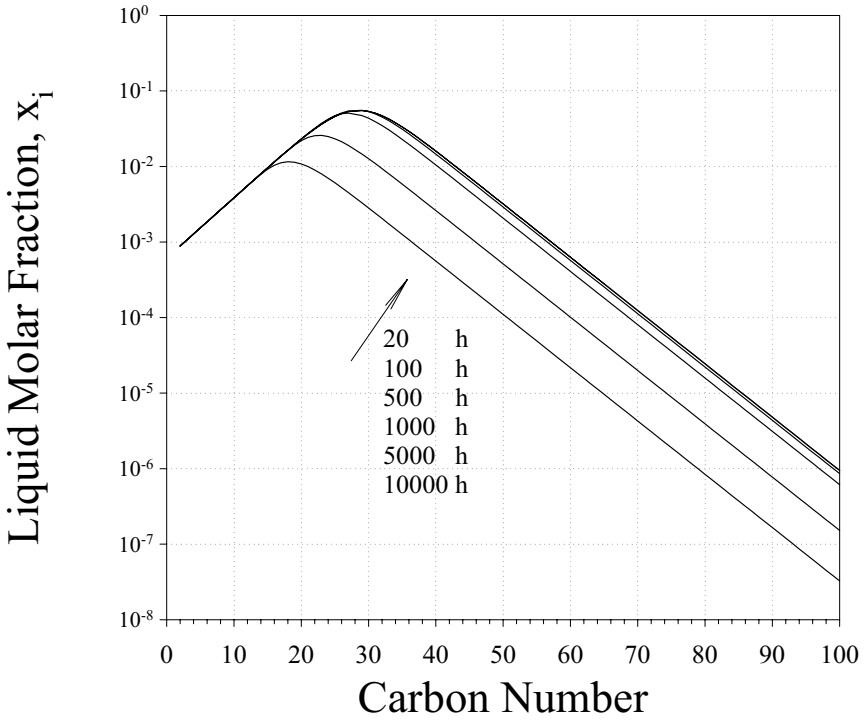

Figure 2 Hydrocarbon molar fraction in Reactor liquid with α=0.85

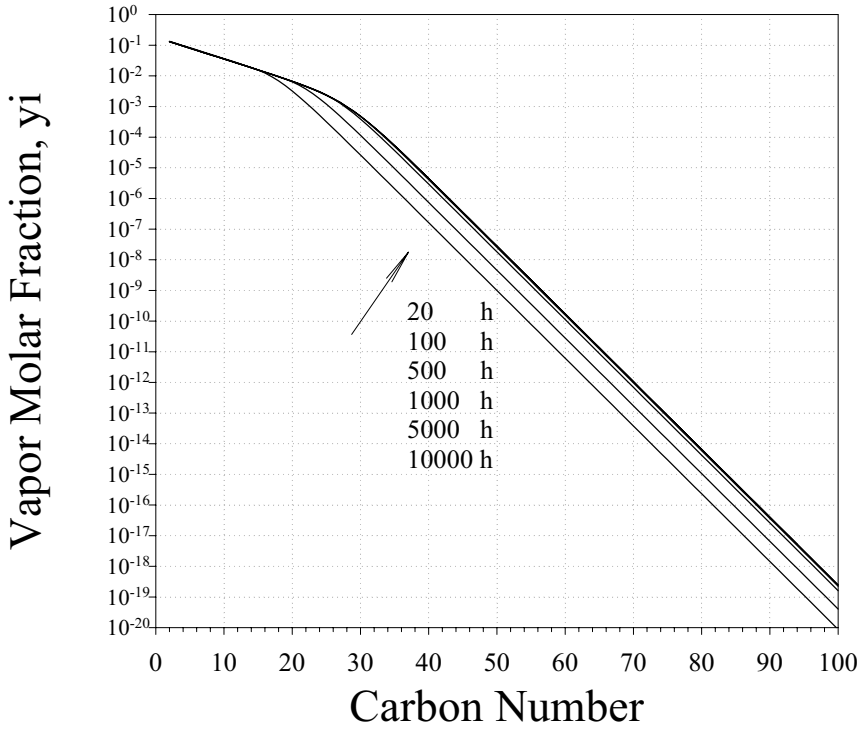

Figure 3 Hydrocarbon molar fraction in vapor phase with α=0.85

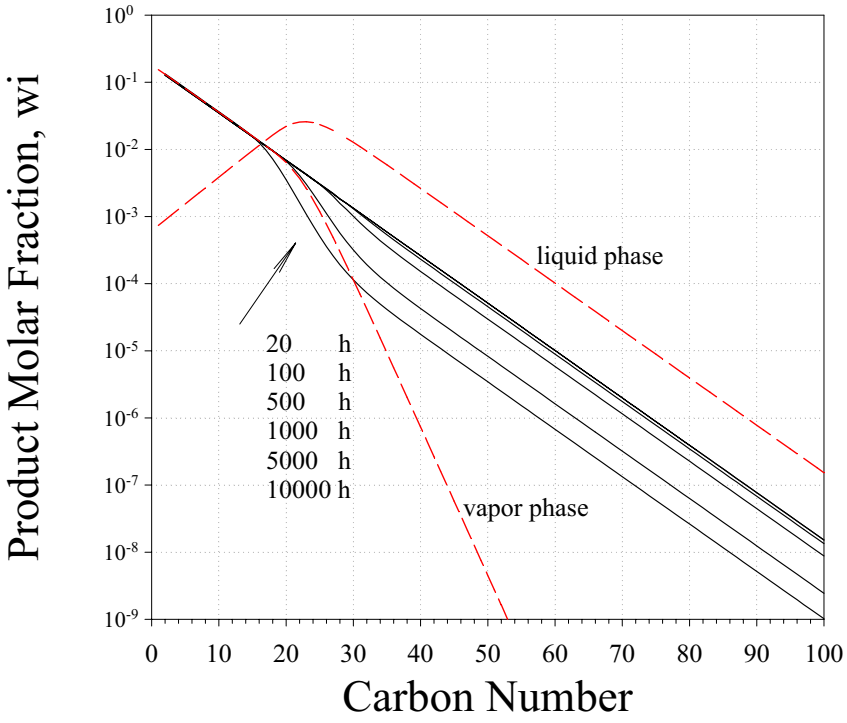

Figure 4 Hydrocarbon molar fraction in total reaction product with α=0.85 (solid line). Dashed lines are liquid phase and vapor phase compositions at 100 h.

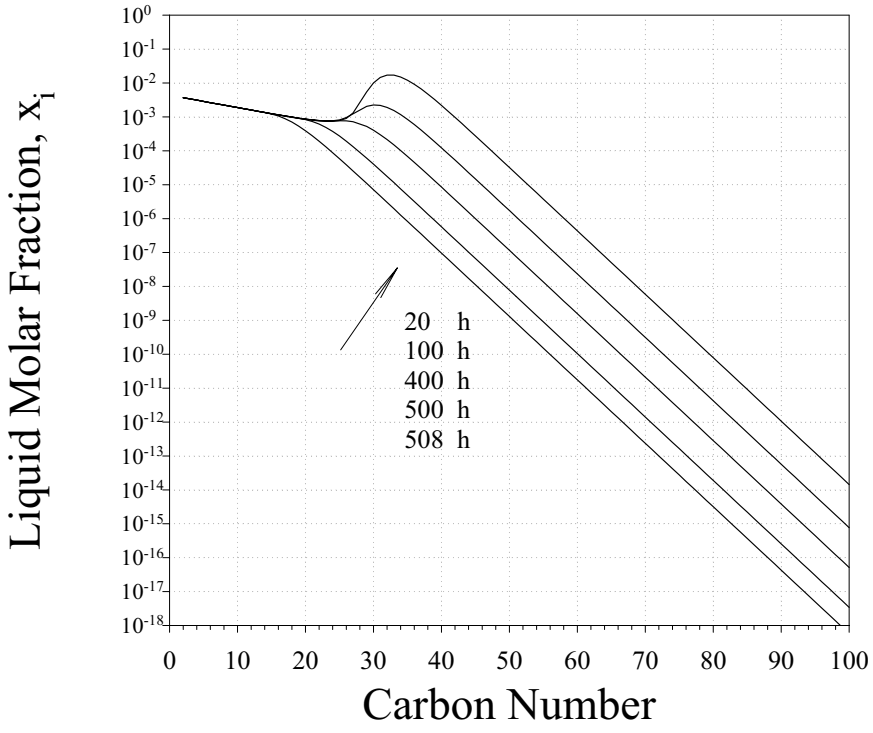

Figure 5 Hydrocarbon molar fraction in liquid phase with α=0.65

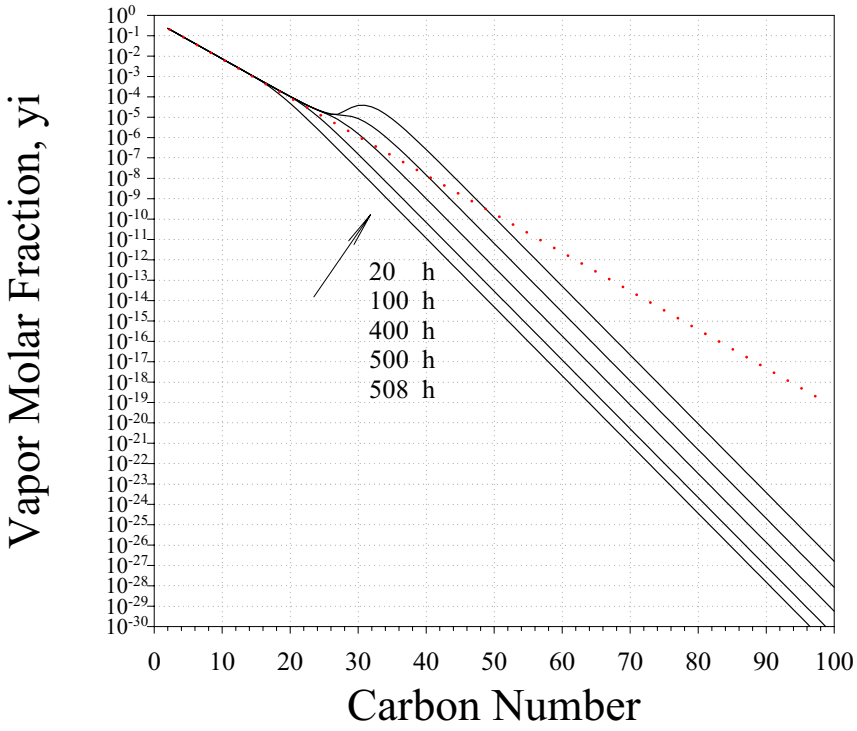

Figure 6 Hydrocarbon molar fraction in vapor phase with α=0.65
(Dotted line is ASF plot)

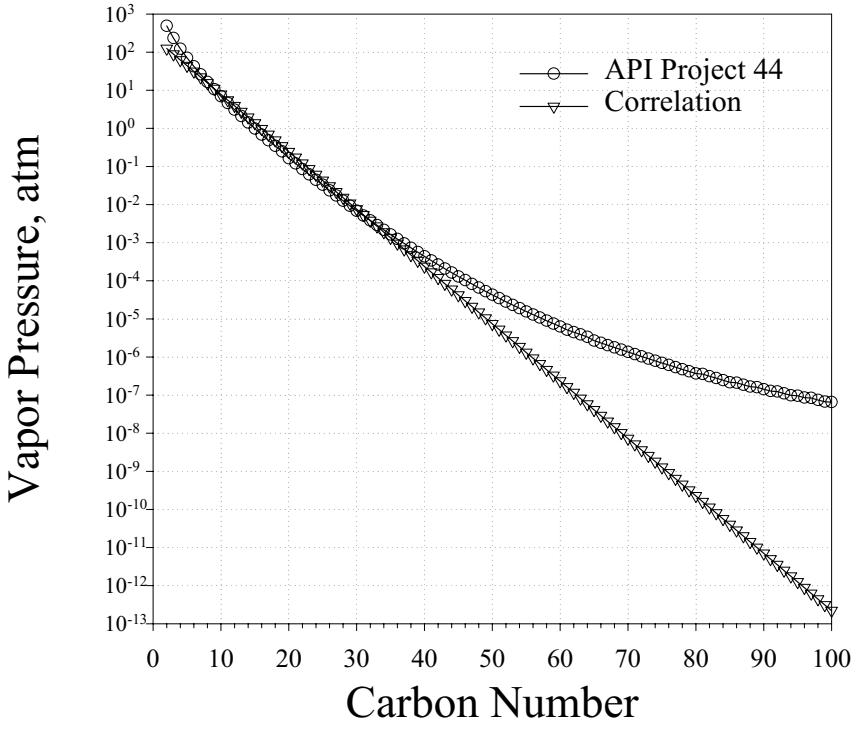

Figure 7 Comparison of paraffin saturation vapor pressure from different sources (270 ^{o}C)

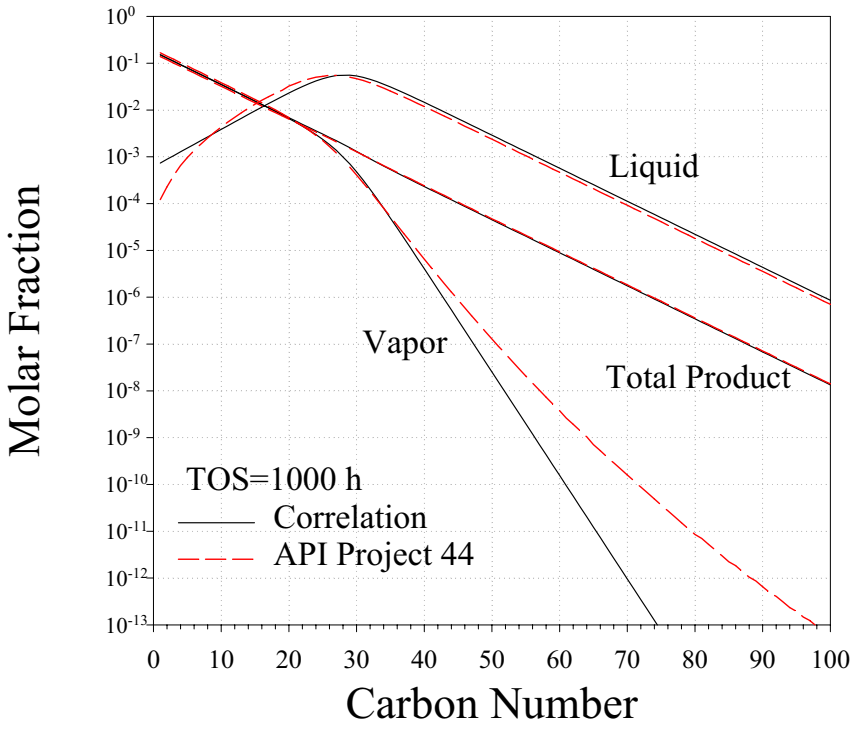

Figure 8 Effect of vapor pressure source on hydrocarbon molar fraction with α=0.85

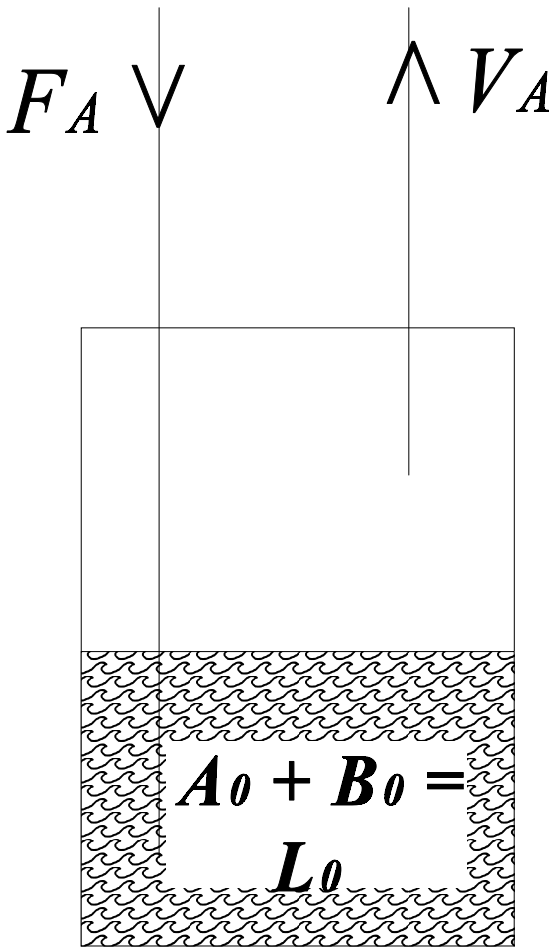

Figure 9. Schematics of a binary separation system.